

## Simultaneous Imaging of Individual Molecules Aligned Both Parallel and Perpendicular to the Optic Axis

Robert M. Dickson,\* D. J. Norris,<sup>†</sup> and W. E. Moerner<sup>‡</sup>

*Department of Chemistry and Biochemistry, University of California San Diego,  
La Jolla, California 92093-0340*

(Received 14 May 1998)

We report the first room temperature observation of an emission pattern from a single fluorescent molecule signifying that the emission dipole is aligned along the optic ( $z$ ) axis of a microscopic imaging system. This technique takes advantage of the  $x$ ,  $y$ , and  $z$ -polarized evanescent fields generated in total internal reflection and the usually nettlesome aberrations commonly encountered when imaging biological samples with high numerical aperture oil-immersion objectives. For both  $z$ -oriented and transverse-oriented individual molecules of the carbocyanine dye DiIC<sub>18</sub> embedded in polymethyl-methacrylate (PMMA), calculated images accurately model the main features of observed emission patterns. [S0031-9007(98)07799-0]

PACS numbers: 42.30.-d, 33.15.Kr, 33.50.-j, 33.80.-b

Complementary to ensemble studies that simultaneously probe many molecules to reveal average properties, single-molecule experiments have the potential to elucidate how each individual molecule interacts with its own surroundings. In recent years, single-molecule optical experiments have lent very useful insights into a wide variety of molecular processes by enabling the direct observation and analysis of normally obfuscated and heterogeneous molecular behavior [1–15]. In such studies, probing each molecule yields time averages instead of ensemble averages of behavior, thus enabling high-contrast observation of fluctuating stochastic processes that are not synchronized in ensemble measurements [7,8,16–21]. Thus, single-molecule studies provide information that, if the experiments are well designed, can facilitate more detailed and precise interpretations in physics, chemistry, and biology, than can ensemble experiments alone. In many instances, especially when relative orientations must be known, careful molecule-by-molecule measurements of three-dimensional molecular orientations can reveal new information on the environmental and intermolecular effects on observed molecular properties. In addition, since the efficiency of important processes such as energy transfer depends on relative orientations of donor and acceptor molecules, the determination of molecular orientation has been a focus of several recent investigations [22–24]. While current single-molecule experiments can measure orientations in the  $x$ - $y$  plane, convenient techniques that fully utilize the three-dimensional orientational information from individual molecules have, to date, not been developed. Although such experiments have the potential to resolve part of the orientational uncertainty in energy transfer experiments, current single-molecule studies are limited by the fact that they are unable to resolve emission dipole moment components along the  $z$  axis [15,22,25]. The uncertainty in the extent of molecular orientation parallel to the optic axis accounts for large sources of

error in single-molecule determinations of intermolecular distances.

Several recent advances have measured the three-dimensional orientations of molecules either with near-field absorption methods or through detailed analysis and interpretation of the molecular emission properties. The near-field method [4] was able to measure the orientation of the *absorption* dipole moment through knowledge of the excitation electric field polarization but was unable to directly resolve the *emission* dipole orientation. Three-dimensional determinations of emission dipole orientations have been performed both by examining the alteration of emission properties due to alignment relative to a dielectric boundary [7,26] and by fitting greatly defocused images of radiating molecules generated in an imaging system employing a low numerical aperture (NA) annular reflective objective [27,28]. While these techniques are useful, they require either thorough lifetime measurements of each single molecule within a given confocal image or reduction of signal to noise for all orientations by defocusing images coupled with postacquisition least-squares fitting.

Here we present a novel single-molecule imaging scheme which simultaneously enables in-focus imaging of molecules oriented in the  $x$ - $y$  plane and defocused imaging of molecules oriented primarily along the optic axis ( $z$  direction; see Fig. 1). This method has the potential to directly image and simultaneously determine the three-dimensional orientation of any highly fluorescent molecule. The technique excites molecules with the  $x$ -,  $y$ -, and  $z$ -polarized evanescent fields generated in total internal reflection (TIR) and collects emission in the presence of aberrations commonly encountered when imaging biological samples. Utilizing this technique, we show for the first time that molecules with emission dipole oriented perpendicular to the optic axis (i.e., lying in the  $x$ - $y$  plane) are observed to be in focus, while molecules aligned along

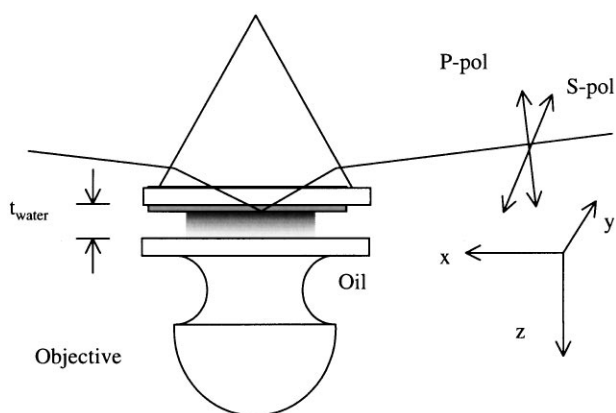


FIG. 1. Experimental setup for simultaneous imaging of  $x$ - $y$ -polarized emission (disk patterns) and  $z$ -polarized emission (doughnut patterns). The evanescent field decays exponentially from the reflecting sample/water interface. The sample is placed on the underside of the upper coverslip and fluorescence is collected from the bottom. Aberrations are introduced upon imaging through a layer of water,  $t_{\text{water}}$ , instead of completely through immersion oil.

the optic axis exhibit out-of-focus emission which has a characteristic ring-shaped “doughnut” profile. Upon incorporating the experimental conditions and aberrations, calculated intensity distributions reproduce the main features of observed emission patterns from highly fluorescent individual carbocyanine dye, DiIC<sub>18</sub>, molecules embedded in polymethyl-methacrylate (PMMA). Individual DiIC<sub>18</sub> molecules in PMMA were spun from a toluene solution onto a glass coverslip according to published procedures [26]. Figure 1 shows a schematic of the experimental setup in which an inverted microscope is used to collect the emitted light. In order to generate the necessary aberrations, a  $\sim 10 \mu\text{m}$  thick layer of water was placed between the coated upper coverslip and an uncoated lower coverslip; TIR occurred at the PMMA/water boundary at the upper coverslip, and the pumping laser radiation extends  $\sim 150 \text{ nm}$  into the water. As is well known, one can adjust the relative  $x$ ,  $y$ , and  $z$  components of the TIR-generated evanescent field by adjusting the angles of incidence and polarization [29,30].

In the images presented here,  $p$ -polarized continuous wave laser excitation at 532 nm undergoing TIR produced  $z$ - and  $x$ -polarized evanescent intensities in a 6:1 intensity ratio, respectively.  $s$ -polarized incident light, however, produced pure  $y$ -polarized excitation of the molecules. Molecular emission was imaged with a  $\text{NA} = 1.4$  oil-immersion objective. A long-pass filter blocked any scattered pumping radiation, and the image was recorded with a Princeton Instruments intensified PentaMax CCD camera. Single molecules observed under these excitation conditions showed a distribution of spots and rings in the image resulting from in-focus and out-of-focus emission. Below we show that molecules oriented in the  $x$ - $y$  plane yield in-focus spots, while those aligned along the optic axis exhibit large aberrations and appear out of focus. For

example, in Fig. 2(a) with two molecules in the same field of view, one (upper left) yields a standard Airy intensity pattern while the other (lower right) is clearly out of focus, exhibiting a doughnut mode indicative of  $z$ -polarized emission. However,  $s$ -polarized excitation produced a purely  $y$ -polarized evanescent field and yielded only in-focus fluorescence signals, i.e., simple localized spots with no central minimum. Figure 2(b) shows another frame of the same region as Fig. 2(a), in which the previously  $z$ -oriented molecule has rotated to an orientation perpendicular to the optic axis—no central minimum in the emission pattern is observed. This motion occurred during the relatively long (0.5 sec) observation time, leading to the departure of the emission pattern from calculated values. Figure 2(c) shows examples of the ring-shaped doughnut structure observed for ten other  $z$ -oriented single molecules. Very sensitive to exact thicknesses of the water and coverslip layers and to rotational motion of the fluorophores, observed emission pattern asymmetries [Fig. 2(c)] may potentially provide more detailed three-dimensional information than that elucidated here.

To analyze these images, we first consider the effect of the optical system on an isotropic point source of light.

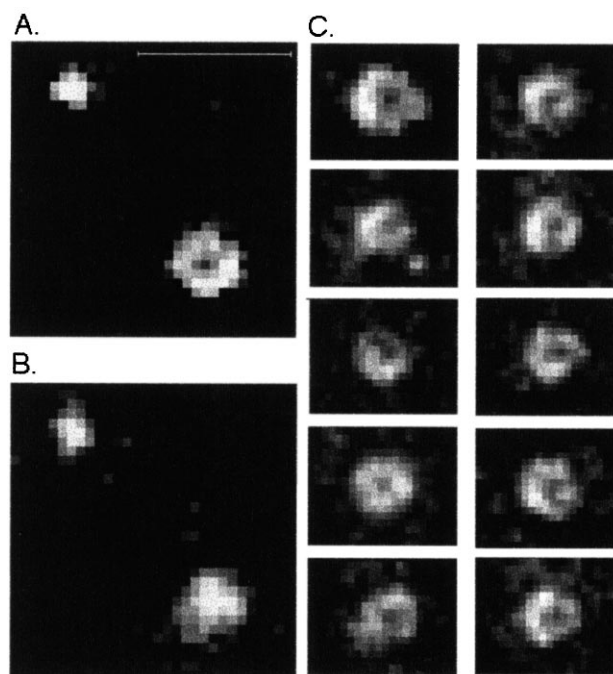


FIG. 2. Images of the emission from single DiI molecules embedded in PMMA. (a) Simultaneous imaging of molecular emission dipoles oriented perpendicular to the optic axis (upper left) and along the optic axis (lower right). These same molecules in (b) show some rotational mobility at the polymer surface as the lower molecule is seen to reorient from being parallel to being perpendicular to the optic axis. (c) Many different single molecules exhibit this doughnut-shaped emission pattern when observed in this imaging scheme. All images are 0.5 sec exposures and are presented with the same gray scale. The scale bar in (a) corresponds to  $1 \mu\text{m}$  in the object plane.

Because of the difference in the refractive index between oil and water, imaging samples through a layer of water with high NA oil-immersion objectives leads to an angle-dependent difference in optical path lengths. This results in the fact that light emanating from the same point source will exhibit a back-focal-plane distance that is collection-angle dependent. Such path length differences give rise to interference at the limiting aperture and produce a resulting intensity distribution that differs significantly from that of the standard Airy point spread function. Upon imaging through a layer of water instead of completely through immersion oil, the optical path difference (opd) as a function of normalized aperture,  $\rho$  ( $\rho = r/r_{\max}$ , where  $r$  is the radius), is given by [31]

$$\text{opd}(\rho) = -n_{\text{oil}}t_{\text{water}}\sqrt{1 - \left(\frac{\text{NA}}{n_{\text{oil}}}\rho\right)^2} + n_{\text{water}}t_{\text{water}}\sqrt{1 - \left(\frac{\text{NA}}{n_{\text{water}}}\rho\right)^2} \quad (1)$$

in which  $t_{\text{water}}$  is the thickness of the water layer, and  $n_{\text{oil}}$  and  $n_{\text{water}}$  are the indices of refraction of the immersion oil and water, respectively (see Fig. 1). The net effect of such aberrations is that light collected at large angles is out of focus relative to that collected at small angles.

Single-molecule studies can exploit these aberrations, since a molecular dipole oriented in the  $x$ - $y$  plane emits at much shallower angles than does a molecule with emission dipole oriented along the optic axis. In order to model the observed images in Fig. 2, we calculated the dipole radiation pattern of molecules at a dielectric boundary according to the methods of Hellen and Axelrod [32] and propagated this radiation through the layer of water and then through an optical system with NA of 1.4. By properly incorporating our experimental parameters including total magnification ( $400\times$ ),  $\sim 25 \mu\text{m}$  CCD pixel size, and the angle-dependent optical path difference into the calculation of the expected diffraction-limited emission pattern, we can generate expected single-molecule intensity distributions,  $I(x, y, z)$ , as a function of detector position and aberration from the Kirchhoff integral [29,31]

$$I(x, y, z) = \frac{I_0(\theta, \phi)}{z^2} \left| \int_0^1 J_0\left(ka\rho \frac{\sqrt{x^2 + y^2}}{z}\right) \times \exp[-ik \text{opd}(\rho)] \rho d\rho \right|^2 \quad (2)$$

in which  $x$ ,  $y$ , and  $z$  give the detector position,  $I_0(\theta, \phi)$  is the intensity distribution in Cartesian coordinates of a dipole oriented with polar angle  $\theta$  and azimuthal angle  $\phi$  with respect to the interface normal,  $a$  is the limiting aperture projected on the back image plane of the objective, and  $k = 2\pi/\lambda$  is the wave vector magnitude.

Calculations of the intensity distribution,  $I(x, y, z)$ , at each point on the detector with zero and nonzero optical path differences from Eq. (1) yield unaberrated and aberrated images, respectively.

We first consider a Gaussian point source imaged through  $10 \mu\text{m}$  of water with a 1.4 NA oil-immersion objective. Figures 3(a) and 3(b) show the calculated point spread functions of unaberrated and aberrated point sources, respectively. When aberrations are included, the point spread function consists of a large spot in the focal plane with a maximum intensity in the center.

Turning now to the single-molecule emitter, calculated intensity distributions from Eq. (2) for dipoles imaged through water, oriented perpendicular and parallel to the optic axis are presented in Figs. 3(c) and 3(d), respectively. When aberrations are ignored, calculated molecular intensity distributions yield images indistinguishable from that presented in Fig. 3(a), independent of molecular orientation. In contrast, to unaberrated images, aberrations introduced by imaging through  $10 \mu\text{m}$  of water, instead of through an equivalent thickness of immersion oil, produce intensity distributions that change significantly with dipolar orientation. Fluorescence signals from molecular dipoles oriented in the  $x$ - $y$  plane [Fig. 3(c)] appear as slightly broadened Airy disks, while  $z$ -oriented dipoles [Fig. 3(d)] appear as bright rings with dark centers. The width of these rings is larger than the diffraction limit and is readily observed when imaged on a CCD.

These calculations which predict the simultaneous measurement of in- and out-of-focus molecules confirm that such aberrations enable  $z$ -polarized emission to be observed. Coupled with the fact that excitation with  $s$ -polarization produces only disks while  $p$ -polarized

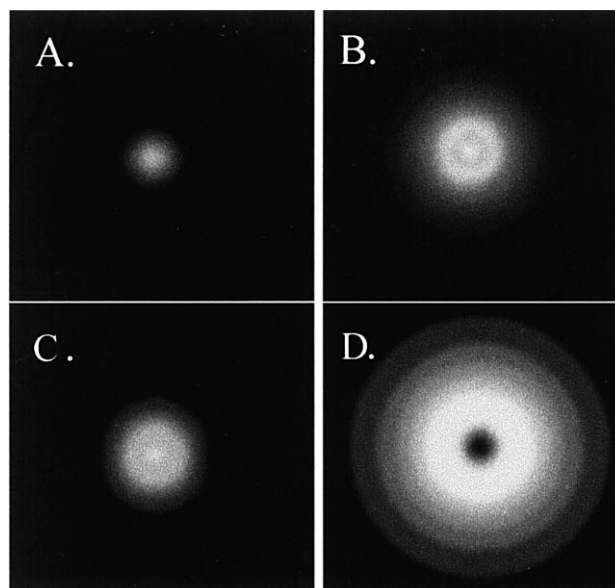


FIG. 3. Calculated intensity distributions. Isotropic Gaussian point source (a) imaged with no aberrations and (b) imaged through  $10 \mu\text{m}$  of water with a 1.4 NA in the object plane. Molecules oriented (c) perpendicular to the optic axis (in the  $x$ - $y$  plane with  $\theta = 90^\circ$ ,  $\phi = 0^\circ$ ), and (d) parallel to the optic axis ( $\theta = 0^\circ$ ,  $\phi = 0^\circ$ ), when imaged through  $10 \mu\text{m}$  water with a 1.4 NA oil-immersion objective.

excitation produces both disks and ring patterns, our results clearly indicate that we are directly visualizing single molecules oriented both perpendicular to as well as along the optic axis. By periodically rotating the laser polarization and analyzing the emission patterns of imaged molecules [22,24], one should be able to further develop these methods to accurately determine the three-dimensional orientations of single molecules at room temperature.

Since the aberrations analyzed in this paper can lead to greatly reduced collection efficiencies when imaging through thick layers of water with high NA objectives, calculation of the correct intensity distributions are particularly important for single-molecule biophysical studies. If properly utilized, however, these aberrations can significantly increase the information obtainable from a given experiment. Recently, polarization-dependent single-molecule techniques have been explored with the goal of understanding individual protein and oligonucleotide behaviors [22,24]. Bulk studies employing fluorescence resonant energy transfer (FRET) are commonly used to probe a wide array of biological processes, but with limiting assumptions about relative chromophore orientations. Such assumptions are less important when utilizing single-molecule FRET techniques [25]; however, it is still necessary to quantify the molecular orientations if distance information is required. In order to conveniently obtain new, relevant information on chromophore orientations, we have employed TIR and image aberrations produced by operation under nonideal conditions, commonly encountered in the study of biological samples. This study provides the first specific experimental results showing how to simultaneously distinguish individual molecules aligned perpendicular to the optic axis from those aligned parallel to the optic axis. Further control of experimental parameters should enable full quantitative determinations of molecular orientations from the shapes of the molecular emission patterns.

The authors gratefully acknowledge partial support from NSF Grant No. DMR-9612252. R. M. D. is grateful for support from NIH Bioengineering and La Jolla Interfaces in Science. D. J. N. was supported by the NSF.

---

\*Present and permanent address: School of Chemistry, Georgia Institute of Technology, Atlanta, GA 30332-0400.  
Email: dickson@chemistry.gatech.edu

†Present and permanent address: NEC Research Institute, Princeton, NJ 08540.

‡Present and permanent address: Department of Chemistry, Stauffer I, Room 15, Stanford University, Stanford, CA 94305-5080.

- [1] T. Basché *et al.*, *Single Molecule Optical Detection, Imaging, and Spectroscopy* (Verlag-Chemie, Munich, 1997).
- [2] W.E. Moerner and L. Kador, *Phys. Rev. Lett.* **62**, 2535 (1989).
- [3] M. Orrit and J. Bernard, *Phys. Rev. Lett.* **65**, 2716 (1990).
- [4] E. Betzig and R. J. Chichester, *Science* **262**, 1422 (1993).
- [5] W.E. Moerner, *Science* **265**, 46 (1994).
- [6] T. Funatsu *et al.*, *Nature (London)* **374**, 555 (1995).
- [7] J.K. Trautman and J.J. Macklin, *Chem. Phys.* **205**, 221 (1996).
- [8] R. D. Vale *et al.*, *Nature (London)* **380**, 451 (1996).
- [9] X. S. Xie, *Acc. Chem. Res.* **29**, 598 (1996).
- [10] J.L. Skinner and W.E. Moerner, *J. Phys. Chem.* **100**, 13 251 (1996).
- [11] W.E. Moerner, *Acc. Chem. Res.* **29**, 563 (1996).
- [12] M.D. Barnes *et al.*, *Phys. Rev. Lett.* **76**, 3931 (1996).
- [13] T. Schmidt *et al.*, *Proc. Natl. Acad. Sci. U.S.A.* **93**, 2926 (1996).
- [14] R. M. Dickson *et al.*, *Science* **274**, 966 (1996).
- [15] A. G. T. Ruiten *et al.*, *J. Phys. Chem. A* **101**, 7318 (1997).
- [16] W.P. Ambrose and W.E. Moerner, *Nature (London)* **349**, 225 (1991).
- [17] P.D. Reilly and J.L. Skinner, *Phys. Rev. Lett.* **71**, 4257 (1993).
- [18] T. Basché, S. Kummer, and C. Bräuchle, *Nature (London)* **373**, 132 (1995).
- [19] R. Brown and M. Orrit, in *Single Molecule Optical Detection, Imaging, and Spectroscopy*, edited by T. Basché *et al.* (Verlag-Chemie, Munich, 1997).
- [20] R. M. Dickson *et al.*, *Nature (London)* **388**, 355 (1997).
- [21] H. P. Lu and X. S. Xie, *Nature (London)* **385**, 143 (1997).
- [22] T. Ha *et al.*, *Phys. Rev. Lett.* **77**, 3979 (1996).
- [23] G. J. Schuetz, H. Schindler, and T. Schmidt, *Opt. Lett.* **22**, 651 (1997).
- [24] T. Ha *et al.*, *Phys. Rev. Lett.* **80**, 2093 (1998).
- [25] T. Ha *et al.*, *Proc. Natl. Acad. Sci. U.S.A.* **93**, 6264 (1996).
- [26] J.J. Macklin *et al.*, *Science* **272**, 255 (1996).
- [27] J. Jasny and J. Sepiol, *Chem. Phys. Lett.* **273**, 439 (1997).
- [28] J. Sepiol *et al.*, *Chem. Phys. Lett.* **273**, 444 (1997).
- [29] M. Born and E. Wolf, *Principles of Optics* (Pergamon, Oxford, 1975).
- [30] D. Axelrod, T. P. Burghardt, and N. L. Thompson, *Annu. Rev. Biophys. Bioeng.* **13**, 247 (1984).
- [31] S. F. Gibson and F. Lanni, *J. Opt. Soc. Am. A* **8**, 1601 (1991).
- [32] E. H. Hellen and D. Axelrod, *J. Opt. Soc. Am. B* **4**, 337 (1987).